7-2002

The Physical Conditions Within Dense Cold Clouds in Cooling Flows - II

Gary J. Ferland
University of Kentucky, gary@uky.edu

A. C. Fabian
University of Toronto, Canada

R. M. Johnstone
Institute of Astronomy, UK

Right click to open a feedback form in a new tab to let us know how this document benefits you.

The Physical Conditions Within Dense Cold Clouds in Cooling Flows - II

The physical conditions within dense cold clouds in cooling flows – II

G. J. Ferland,[1,2] A. C. Fabian[3] and R. M. Johnstone[3]★

[1]*Department of Physics, University of Kentucky, Lexington, KY 40506, USA*
[2]*Canadian Institute for Theoretical Astrophysics, University of Toronto, McLennan Labs, 60 St George Street, Toronto, M5S 3H8, Canada*
[3]*Institute of Astronomy, Madingley Road, Cambridge CB3 0HA*

ABSTRACT

This is a progress report on our numerical simulations of conditions in the cold cores of cooling flow condensations. The physical conditions in any non-equilibrium plasma are the result of a host of microphysical processes, many involving reactions that are research areas in themselves. We review the dominant physical processes in our previously published simulations, to clarify those issues that have caused confusion in the literature. We show that conditions in the core of an X-ray-illuminated cloud are very different from those found in molecular clouds, largely because carbon remains substantially atomic and provides powerful cooling through its far infrared lines. We show how the results of the Opacity Project have had a major impact on our predictions, largely because photoionization cross-sections of atoms and first ions are now calculated to be far larger than estimated previously. Finally, we show that the predicted conditions are strongly affected by complexities such as microturbulence or the presence of small amounts of dust. Large masses of cold dense gas, in addition to the warmer molecular gas detected recently, could be present in cooling flows.

Key words: atomic processes – molecular processes – galaxies: clusters: general – cooling flows – intergalactic medium.

1 INTRODUCTION

Ferland, Fabian & Johnstone (1994; hereafter FFJ) computed the thermal and ionization structure of a constant-pressure cloud embedded within a cooling flow and exposed to radiation from the cooling flow and the cosmic background. By hypothesis the cloud was taken to be free of dust grains. FFJ also computed a conventional dusty Orion photodissociation region (PDR) model as an appendix. FFJ tried to identify the most important physical processes affecting the state of the gas. Any cloud will cool down to the temperature of the cosmic background once it is sufficiently shielded from other sources of radiation. In their calculation they found that this occurred after a hydrogen column density of $4 \times 10^{21}\,\mathrm{cm}^{-2}$.

Several papers have questioned this result, mainly working by analogy with galactic molecular clouds (O'Dea et al. 1994; Braine et al. 1995; Voit & Donahue 1995, hereafter VD; Henkel & Wiklind 1997). Here we reconsider the FFJ calculation and go over some details that may have caused confusion. Any numerical simulation of a non-equilibrium plasma is the result of a balance between a host of microphysical processes. Many of these processes are research areas in themselves, and can have substantial uncertainties. In some circumstances the final results may be sensitive to an especially effective creation or destruction mechanism, and in others to dozens or more channels. On top of

this there may be fundamental questions such as whether the gas is in a steady state.

The purpose of the present paper is to investigate in detail what happens to a cloud that is maintained at a reasonably high pressure ($\sim 10^5\,\mathrm{cm}^{-3}\,\mathrm{K}$) for billions of years and at the same time is continuously exposed to X-ray radiation from the surrounding, pressure-confining medium. In particular, we investigate the physical processes for the coldest parts of the cloud, which enable the temperature to be significantly less than 17 K. Small amounts of microturbulence, or grains, cause it to be much colder still. Calculations by Puy, Grenacher & Jetzer (1999) have also found a low final temperature for a fully molecular cloud in a cooling flow.

2 WHAT HAPPENED IN THE FFJ MODEL

Several questions have arisen concerning the calculation presented by FFJ: (i) why does the cooling function not agree with existing molecular cloud cooling functions; (ii) does the cooling caused by the [C I] 370- and 610-μm lines violate fundamental thermodynamic limits; and (iii) VD point out that the heating efficiencies, taken from Shull & van Steenberg (1985) have been superseded by more recent calculations (Xu & McCray 1991), which do not agree for very low-electron fractions.

In this section we use an early version of CLOUDY (C84.09) to recompute the model shown in FFJ to illustrate some of the dominant physics. We believe that this is the version used for that work.

★E-mail: rmj@ast.cam.ac.uk

2.1 Cooling flow cloud versus molecular cloud cooling functions

The cooling functions computed for molecular clouds by Goldsmith & Langer (1978), used by O'Dea et al. (1994) and Braine et al. (1995), do not agree with FFJ. In particular, O'Dea et al. (1994) predict a temperature of between 30 and 50 K. Examination of the original papers reveals the problem. The FFJ model has no dust, which greatly reduces the H_2 formation rate. Also carbon remained mostly atomic across the cloud (fig. 2 in FFJ). This was caused by rapid charge transfer, $CO + He^+ \rightarrow O + C^+ + He$, well known to be the dominant CO destruction process in most environments (Tielens & Hollenbach 1985a). He remains partially ionized because of the low-electron density, its large photoelectric cross-section at X-ray energies, and significant abundance of suprathermal electrons from X-ray photoionization.

This situation is totally unlike that assumed in calculations of the molecular cloud cooling function. There, cooling caused by atomic carbon is assumed to be a minor component. For an environment where C/O < 1 little atomic carbon will exist when the gas becomes totally molecular and all C is locked up in CO. The difference between FFJ and molecular cloud cooling functions is the contribution of [C I] cooling, which can be intense.

VD present separate curves for the cooling caused by CO and [C I]; our result agrees with that of VD for neutral atomic gas, i.e. where the major low-temperature coolant is [C I].

2.2 The blackbody limit to [C I] emission

The [C I] 370- and 610-μm lines were especially important coolants in the calculation of FFJ. Their fig. 3 shows that these lines dominated the cooling beginning from a depth of roughly 1.5×10^{16} cm (3×10^{19} cm^{-2}) and extend to the point where CO was the dominant coolant. The temperatures over this region were below roughly 15 K. The issue here is whether the emergent intensity of the [C I] lines violates fundamental thermodynamic limits.

For a cloud with constant source function S_ν, the emergent specific intensity is trivially given by $I_\nu = S_\nu[1 - \exp(-\tau)]$. For a thermalized line, for frequencies near the line centre S_ν is the Planck function at the excitation temperature, and we obtain the familiar result that the intensity saturates at the blackbody intensity. The astrophysical flux $\mathcal{F}_\nu$ (Allen 1973, p. 90) is then πB_ν and the one-sided emittance, or energy emitted by a cloud into 2πsr, will be $\pi B_\nu \delta\nu$.

FFJ gave the total emittance or total energy emitted by both sides of a cloud into 4πsr. The blackbody limit, for the plane-parallel approximation, is $2\pi B_\nu \delta\nu$. For $\delta\nu$ we take the full width at half maximum for the [C I] 610-μm line. It has an optical depth of roughly 80, so the line is optically thick to 2.09 times the Doppler core (Elitzur & Ferland 1986).

The cloud computed by FFJ was not isothermal, and it is not possible to determine at what temperatures the emergent [C I] 610-μm line was produced, given the figures shown. FFJ did show the fraction of the total cooling carried by the lines, and the lines dominated the cooling at depths of between 1.5 and 5×10^{16} cm. It is important to remember that heating and cooling balance one another, and that the heating rate falls drastically across the cloud as the incident continuum is attenuated. The statement that the line is a uniformly major contributor to the cooling between these depths is not equivalent to the statement that these depths are the dominant contributors to the total emittance.

Figs 1(a) and (b) show the temperature structure (upper panel)

and local emissivity over the regions where the [C I] fine structure lines form. The [C I] 610-μm line forms predominantly within a narrow region near 1.4×10^{16} cm. The emissivity-weighted mean temperature where the 610 μm line is formed is 27.5 K, and the total emittance for a blackbody at this temperature and linewidth is 1.3×10^{-5} erg cm^{-3} s^{-1}. The total emittance predicted by FFJ was substantially less at 2.1×10^{-6} erg cm^{-3} s^{-1}.

Although Fig. 1(b) shows that the emissivity of the 610-μm line has a tail that extends to substantially cooler temperatures, we confirm that the emissivity in this line does not exceed the blackbody limit at any point within the cloud.

We note that the geometry assumed by the CLOUDY code is appropriate for a cloud in the outer parts of a cooling flow (say at
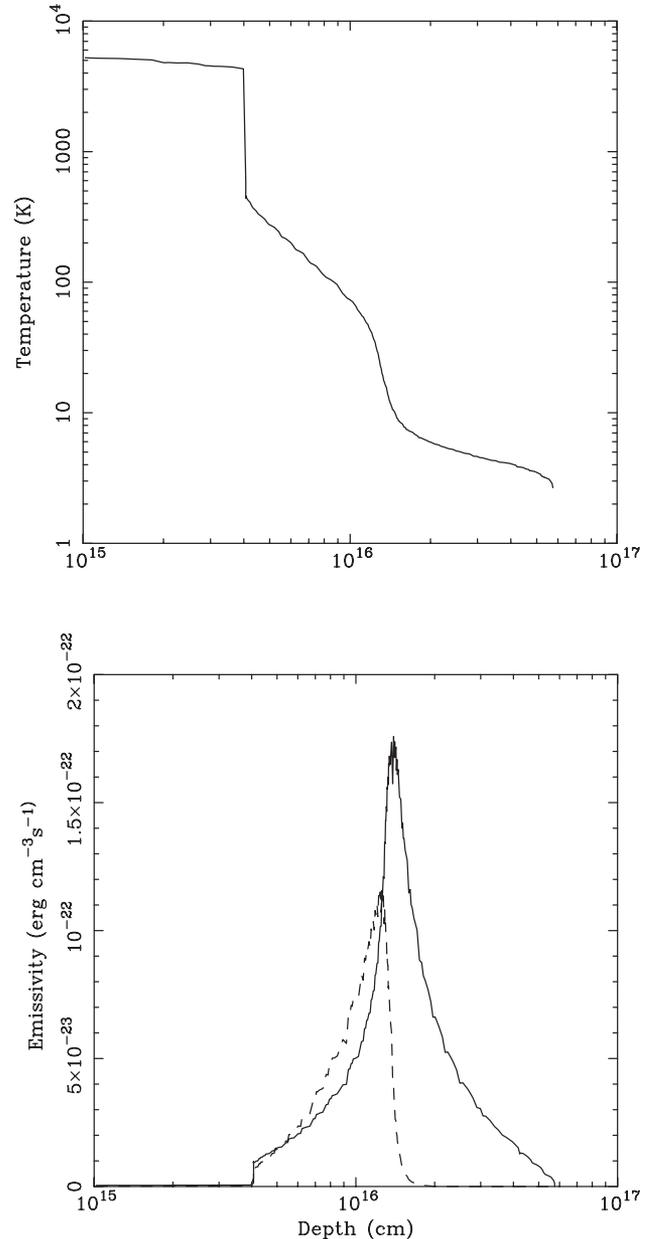
Figure 1. For the model computed in FFJ, using C84.09. (a) Upper panel: electron temperature as a function of depth into the cloud. (b) Lower panel: emissivity of [C I] 370 μm (dashed) and 610 μm (solid) lines as a function of depth into the cloud.
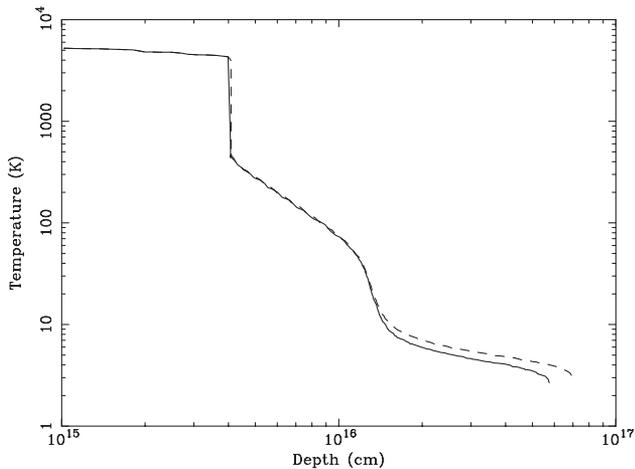
Figure 2. Temperature structure of the constant-pressure cloud, using the X-ray heating rates of Shull & van Steenberg (solid line) and Xu & McCray (dashed line), both in C84.09.

100-kpc radius, which is that assumed by FFJ). The radiation from the cooling flow is incident on one face; the other, cold face, is exposed to deep space and the microwave background. This will be inappropriate for clouds near the centre of the flow. Since they are heated from all sides it is plausible that the inner cores of such clouds are warmer than calculated here and we consider this geometry below. We note that both cold and warm clouds are commonly seen in the central regions of cooling flows.

## 2.3 Revised low-ionization fraction heating efficiencies

In an ionized gas all photoelectrons have their energy converted to thermal energy by rapid elastic collisions with free electrons. In a predominantly neutral gas, X-ray photoelectrons heat, excite and ionize the gas before they are thermalized. FFJ used the fits of Shull & van Steenberg (1985) to Monte Carlo calculations to take these effects into account. VD point out that the more recent calculations of Xu & McCray (1991) show that these fitting formulae do not have the proper asymptotic limit. This affects regions with electron-to-hydrogen atom ratios of less than 10^{-4}. Regions of the cloud modelled by FFJ deeper than $\sim 1.5 \times 10^{16}$ cm (or with a hydrogen column density greater than 3×10^{19} cm^{-2}) do have electron fractions smaller than this.

Fig. 2 shows that the effects of changing from the results of Shull and van Steenberg to those of Xu and McCray do indeed affect the results by a modest amount, and make the core of the cloud warmer.

3 ADVANCES IN THE MICROPHYSICS

Any simulation of a non-equilibrium plasma rests on a foundation of a host of microphysical processes. Estimates of rates and cross-sections have improved enormously over the past decade, some of which are relevant to the problem addressed here. CLOUDY has been revised to take account of these advances. Version numbers are used to track the changes and the CLOUDY home page http://www.pa.uky.edu/~gary/cloudy records them in detail. FFJ used version C84.09 of the code. That version had rates and cross-sections that were up-to-date *c*. 1992. The current version is C96 and every effort has been made to update the entire atomic–molecular data base to the best current values (Ferland et al. 1998).

As we show below, the physical conditions predicted by the two
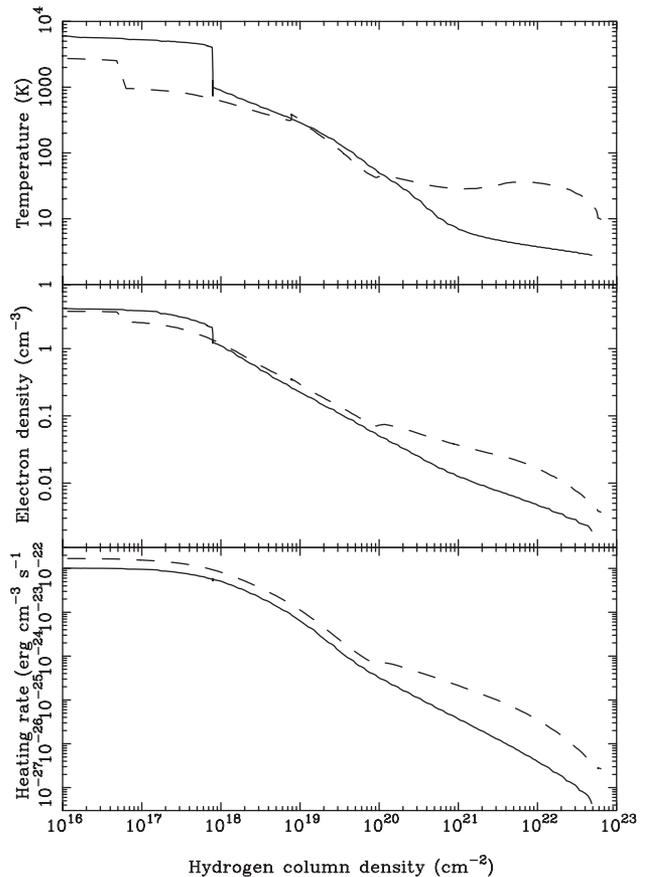
Figure 3. Comparison between CLOUDY version 84.09 (solid) and 90.04 Dashed). Note that these models are for the case of constant-density clouds (see Section 3 for the reason for this) and not the constant-pressure clouds computed by FFJ.

versions of the code do not agree deep within the cooling-flow-irradiated cloud. Here we identify the physical processes that have caused the computed conditions to change. We will compare an existing copy of version 84.09 (after correcting for the proper asymptote for the secondary ionizations) with the version of the code now available on the web.

3.1 Constant-density model

The original FFJ calculation used a constant-pressure cloud. This was motivated by the physical situation, visualized as one in which the hot X-ray-emitting plasma and the cool clouds are at pressure equilibrium. For this comparison between the two versions we consider constant-density clouds to clarify the real differences in the codes. The constant-pressure assumption exaggerates differences between similar photoionization models, since minor differences in the thermal structure are magnified by resulting changes in the density and ensuing opacity. Otherwise the initial conditions are identical to FFJ. In particular, we will stop both calculations at the same column density, $\log(N_{\rm H}) = 22.8$ cm^{-2}. This is the depth at which the temperature predicted by C84.09 fell below 4 K.

3.1.1 Conditions at the illuminated face of a cloud

Fig. 3 shows some details of the FFJ standard cloud computed by both C84.09 and the current version. The electron temperatures at

the illuminated face differ by significant amounts, with the current version being cooler. Temperature is the result of the balance between heating and cooling. Fig. 3 also shows that the photoelectric heating is nearly the same at the illuminated face.

The differences at the illuminated face are caused by changes in the cooling efficiency of the gas. The biggest change is caused by infrared (IR) lines within the ground term of Fe^+. The current version of the code uses collision strengths from Zhang & Pradhan (1995). The [Si II] 34-μm line is stronger now; the current version uses the recent collision strengths from Dufton & Kingston (1994). None of these rates were available for C84.09. Changes in the charge transfer data base, especially reactions involving He and He^+ (Wang et al. 2001, in preparation; http://www-cfadc.phy.ornl. gov/astro/ps/data/), also increased the cooling by changing the ionization of the gas. Fe was predicted to be ∼ 50 per cent in the form of Fe^+ in the old calculation, while close to 100 per cent of Fe is now predicted to be in the form of Fe^+. This further increases [Fe II] cooling and results in lower temperatures. The result of this increased cooling efficiency is that the gas now equilibrates at a somewhat lower temperature (2700 K) than it did in version 84 (6380 K). The gas pressure is smaller by the corresponding factor.

The figure also shows that the depth at which the thermal front, where the gas abruptly changes from the warm (∼ 4000 K) to cool (< 1000 K) phases, is also different. This is again caused by changes in the details of the cooling function.

### 3.1.2 Conditions deep within a cloud

Fig. 3 shows that the largest differences occur deep within the cloud. The photoelectric heating is now roughly a factor of 2 larger, as is the electron density and the resulting temperature. These differences are caused by two major improvements in the atomic data base.

Fig. 4 shows the local continuum at the shielded face of the cloud. The dashed line is the incident continuum produced by the surrounding cooling flow. The solid line is the continuum predicted by the later code, and the dotted line is that predicted by C84.09. (These continua are in excellent agreement, and the two are often not distinguishable.)

The continuum is strongly absorbed between the atomic carbon edge (11.2 eV) and several keV. Rayleigh scattering provides significant additional shielding for energies longward of Lyα. The net effect is that the conditions deep within the cloud are determined by gas interactions with both very soft (5–10 eV) and very hard (> 2 keV) radiation.

The entire photoionization cross-section data base was revised in C90 (Ferland et al. 1998). C84.09 used photoionization cross-sections computed by Reilman & Manson (1979). The physical assumptions they used were very accurate for highly charged species, but became increasingly approximate for lower charges. The data base used in C96 is described by Verner et al. (1996). It uses experimental or Opacity Project (Seaton 1987) cross-sections and gives partial cross-sections explicitly for each subshell. The Reilman & Manson and the Verner et al. data sets are in good agreement for second and more highly charged ions, and for the inner shells of most ions, but are quite different for valence shells of atoms and first ions. A comparison of the opacity between 0.1 and 3 Ryd computed by C84.09 and the later code is shown in Fig. 5.

Deep in the cloud there is actually more power available in reprocessed Balmer continuum radiation than in the attenuated X-ray continuum (Fig. 4). This cloud has a very low level of
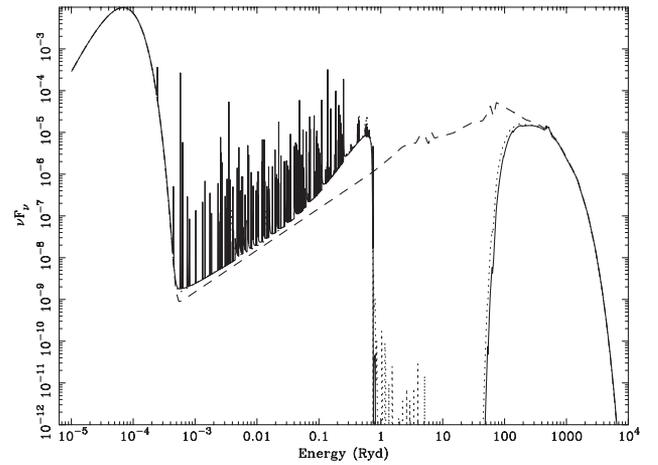
Figure 4. Comparison of spectra for the constant-density models. Dashed line: incident flux. Solid line: flux at shielded face of cloud predicted by the later code. Dotted line: flux at shielded face of cloud predicted by C84.09.
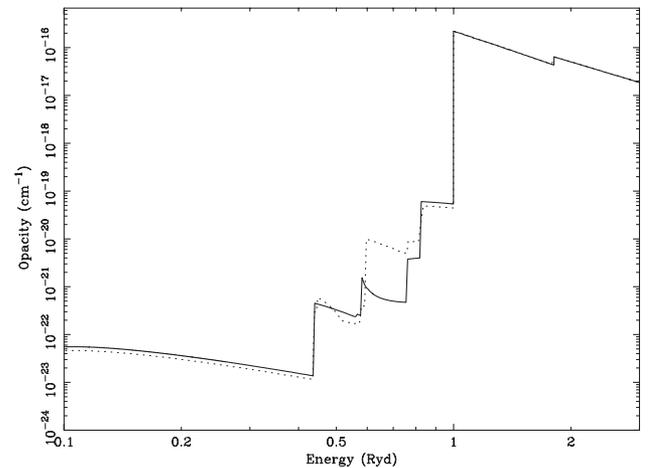
Figure 5. The predicted total opacity at the illuminated face of the cloud for C84.09 (dashed line) and C96 (solid line).

ionization, and there have been dramatic increases in the photoionization cross-sections for neutral atoms and first ions. The valence-shell photoionization cross-sections for atoms and first ions are now often 0.5–1.0 dex larger. Fig. 5 shows that the total gas opacity, as determined by these cross-sections and the resulting ionization balance, also differs by up to 1 dex. This results in substantially different photoionization rates, photoelectric heating, and electron densities, mainly caused by third-row elements with small ionization potentials (Na, Si, S, Ca). These species were atomic in the C84.09 solution, but are predicted to be first ions by C96. This accounts for roughly half of the differences between the two calculations.

The remaining differences are largely caused by changes in the fluorescent yields and distribution of Auger electrons. Version 84 used the approximate methods outlined by Weisheit & Dalgarno (1972), Weisheit (1974) and Weisheit & Collins (1976). The current version employs the extensive data set of Kaastra & Mewe (1993), combined with detailed subshell photoionization cross-sections (Verner et al. 1996). The distribution of Auger electrons ejected for third- and fourth-row elements is significantly different. The resulting equilibrium is especially sensitive to

details of inner-shell processes since an exceptionally hard continuum is present at depth (Fig. 4).

The net result is that the gas is more highly ionized with larger photoelectric heating rates. It is unusual for a calculation to change by as much as this one has, because changes in the atomic data base tend to be random and so have a small net effect. In this case the changes in the valence-shell photoionization cross-sections and numbers of Auger electrons have all been in the sense to result in increased ionization and heating, and they have had a major net effect.

3.2   Changes to molecules and grains

A major effort has gone into making the grain physics state-of-the-art. The current implementation is described by van Hoof et al. (2001). A built-in Mie code can be used to generate optical properties for any grain constituent, and the grain population can be resolved into any number of size bins. Grain charging, heating, temperature and drift velocity is then computed for each size. Resolving the grain size distribution is crucial since smaller grains tend to be hotter, produce the greatest photoelectric heating of the gas, and so have a profound effect on the spectrum. Polycyclic aromatic hydrocarbon (PAH) and single-photon heating (Guhathakurta & Draine 1989) are also fully treated. The current implementation of the grain physics fully reproduces the results presented by Weingartner & Draine (2001), but with the added advantage of including a self-consistent solution of the physical state of the gas surrounding the grains (radiation field, electron kinetic energy distribution, etc.).

The molecule network presently includes H^-, H_2, H_2^+, H_3^+, HeH^+, OH, OH^+, CH, CH^+, O_2, O_2^+, CO, CO^+, H_2O, H_2O^+, H_3O^+ and CH_2^+. Reaction rate coefficients are from Hollenbach & McKee (1979, 1989), Tielens & Hollenbach (1985a, 1990), Lenzuni, Chernoff & Salpeter (1991), Wolfire, Crosas & Weisheit (1993), Puy et al. (1993), Maloney, Hollenbach & Tielens (1996), Hollenbach & Tielens (1999), and the UMIST data base (http://www.rate99.co.uk/). The resulting chemistry is in good agreement with standard PDR calculations. The effects of suprathermal electrons are important and treated as in Dalgarno, Yan & Liu (1999).

CO includes both $^{12}C^{16}O$ and $^{13}C^{16}O$ using shielding rates from van Dishoeck & Black (1988) and all radiative transfer processes. These molecules are treated as rigid rotators with a complete calculation of the level populations and emission from the ground rotational ladder. Any number of levels can be included; the current calculation includes the lowest 50 levels and uses collision rates from de Jong, Chu & Dalgarno (1975). The older calculation treated CO rotation cooling using expressions from Hollenbach & McKee (1979). This is crucial for the cloud cores, where CO is the dominant coolant. The current calculations obtain the CO cooling by solving for level populations along the full rotational ladder, including collisional excitation, de-excitation, continuum pumping excitation and line trapping. This treatment is expected to be more rigorous because it is evaluated at each point for the detailed local conditions and line optical depths for lines along the CO rotational ladder. Tests show that the cooling predicted by the detailed molecule is generally within a factor of 3 of that predicted by the approximation of Hollenbach & McKee. Besides its greater accuracy, another benefit of the complete model molecule is that the full rotation spectrum is predicted. The work of Puy et al. (1999) considered the cooling function due to molecules of H_2 CO and HD. We have checked and found that the inclusion of the HD molecule has no significant effect on our results.
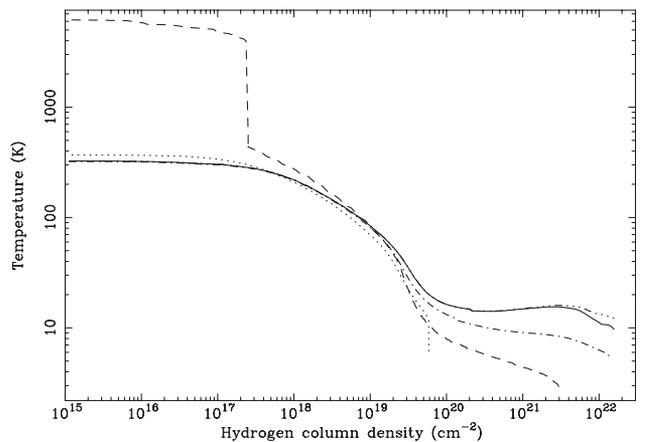
Figure 6. Temperature profiles within the irradiated clouds. All models assume constant pressure and have the same outer pressure of 2.9×10^5 cm^{-3} K. Solid line: C96, no microturbulence, no dust. Dashed line: C84.09, no microturbulence, no dust. Dot-dashed line: C96 with 1 km s^{-1} microturbulence, no dust. Dotted line: C96, no microturbulence, galactic dust-to-gas ratio. The triple-dotted-dashed curve depicts the cloud illuminated from all sides.

3.3   Constant pressure model

Johnstone, Fabian & Taylor (1998) recalculated the FFJ cold cloud model using C90.04, and found that there existed an extended region in the core of the cloud with a temperature of between 13 and 17 K at column densities up to 4×10^{21} cm^{-2} (their fig. 8). In Fig. 6 we show the temperature profiles within the clouds for C84.09 (dashed line) and C96 (solid line). The reasons for the difference in the models between versions are as explained in Section 3.1.

4   WHAT HAPPENS IN NATURE?

4.1   Equilibrium time-scales

FFJ's calculations were basically of a conventional photodissociation region. They presented both a grain-free model of a constant-pressure cooling flow cloud and, as an appendix, the dusty Orion blister. The methods and assumptions they used were based on the chemistry that occurs in conventional PDR (Tielens & Hollenbach 1985a,b) and warm shocks (Hollenbach & McKee 1979, 1989). Where comparisons were possible the calculations obtained by FFJ using the then current version of the code CLOUDY were in reasonable agreement with these papers. The assumption that the structure has had time to come into time-steady equilibrium underlies all of this work. FFJ did check that the recombination and thermal time-scales were short.

Since that time Draine & Bertoldi (1996) have shown that, even for conventional galactic objects such as the Orion PDR, the H_2 part of the chemistry is so slow that it may not reach equilibrium (Bertoldi & Draine 1996; Draine & Bertoldi 1996). The basic reason is that for a homonuclear species such as H_2 direct formation is not possible (there is no dipole moment) and only indirect mechanisms are available. In the case of H_2 these include radiative association through H^- and catalysis on grain surfaces. For a grain-free environment only the first process is possible.

CLOUDY (C96) now checks time-scales for most important parts of the ionization and thermal solutions. Fig. 7 shows some of these time-scales for the FFJ cloud. This calculation is of a constant-
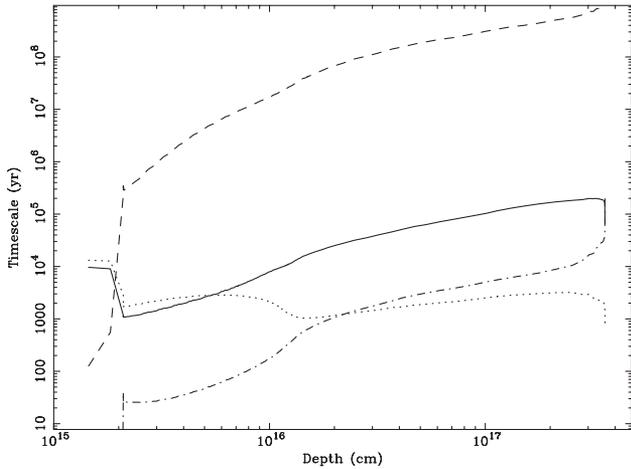
Figure 7. Equilibrium time-scales for cooling (solid line), H_2 molecule formation (dashed line), CO molecule formation (dot-dashed line) and recombination (dotted line) as a function of depth into the cloud.

pressure cloud with the density at the illuminated face given in FFJ. Time-scales for recombination, thermal equilibrium and the formation of the important species CO and H_2, are shown. All time-scales are fast enough for them to reach steady state. At the shielded face of the cloud the longest time-scale is that for H_2 formation, but even here the time-scale of ~ 1 Gyr is probably fast enough to have reached equilibrium. The major effect of the H_2 network being out of equilibrium would be to introduce an uncertainty in the total hydrogen density since the H and H_2 fractions are uncertain. H_2 has little influence on the thermal balance of the cloud, however.

4.2 Dependence on the velocity field

One parameter that strongly affects the results is the local velocity field. The original calculation was of a cloud at pressure equilibrium with its surroundings. Only thermal line broadening was assumed. We have now computed the temperature structure of the constant-pressure cloud using C96 and including a micro-turbulent velocity field of $1 \, \mathrm{km \, s^{-1}}$. (This is the Alfvén speed of a matter-dominated magnetic field that has an energy density of only 0.02 per cent of the thermal energy density at the illuminated face of the cloud. This would be unusually low in the interstellar medium of our Galaxy.) The only physical effect of the micro-turbulence is to desaturate the lines and allow them to cool more efficiently. The dot-dashed line in Fig. 6 shows the temperature profile resulting from this model; temperatures are approximately a factor of 2 cooler at depth. Since the thermal width for the [C I] fine structure lines is only a fraction of a kilometre per second, even modest levels of turbulence have a substantial effect. Most of the core of a realistic, dust-free cloud is therefore below 10 K.

4.3 Dependence on the presence of dust

Grains have a dramatic effect on the structure of these clouds. Fabian, Johnstone & Daines (1994) and more recently Johnstone, Fabian & Taylor (1998) showed the effects of a variety of dust-to-gas ratios on the temperature profiles of the clouds. We reproduce the model from Johnstone, Fabian & Taylor, which included dust at the galactic gas-to-dust ratio as the dotted line in Fig. 6.

In the calculations with dust absent the gas had essentially no opacity in the Balmer continuum. H_2 formation proceeded only

through the H^- route. At depth the radiation field was dominated by reprocessed Balmer continuum radiation. This radiation field dominated the physical conditions there.

In the dusty model the H_2 and CO molecular fractions are far larger than in the grain-free case; both approach 100 per cent of the H or C abundance. H_2 forms more efficiently on grain surfaces, and the added grain opacity shields H_2 and CO from photodissociating radiation. The grain opacity peaks at energies near 1 Ryd, so the grains become a significant part of the ionizing radiation field. The biggest effect of this is that the reprocessed Balmer continuum is approximately a factor of 20 weaker in the dusty case. There is therefore far less heating of the gas at depth and the cloud reaches the background temperature at a column density of just over $10^{20} \, \mathrm{cm^{-2}}$. The [Si II] and [Fe II] emission lines are predicted to be much weaker than in the non-dusty case caused by depletion of these elements on to dust grains.

We have considered the effect that the ambient galaxy starlight has on the structure of our cloud by modelling it as a stellar atmosphere (Kurucz 1991) with $T_{\mathrm{eff}} = 4500 \, \mathrm{K}$. We set the stellar flux incident on the cloud by assuming the starlight from the whole galaxy was a point source with an absolute bolometric magnitude of -23, located at a distance of 100 kpc from the cloud. There is no discernible difference in the temperature structure of the cloud when this radiation field is included. We note that on smaller scales, in the central regions of cooling flow galaxies, there is evidence for excess blue light that may power the optical emission line regions (Johnstone et al. 1987; Allen 1995; Crawford et al. 1995).

4.4 Cloud irradiated from all sides

As mentioned above, the models we consider are appropriate for condensations in the outer regions of the flow, where diffuse emission from the hot gas strikes only one face of the cloud we model. The shielded face is exposed only to the extragalactic background radiation. The cloud is able to freely radiate in this outer direction, which is also the coldest part of the cloud.

For regions closer to the centre of the flow, a cloud will be illuminated from all sides. In this case the most shielded region will be the core of the cloud, which will not be able to radiate very efficiently because of the shielding effects of the surrounding gas. How does this warmer layer of gas affect the core temperature? As VD point out, in the simple case of a cloud cooled only by one optically thick line, the temperature of the core could not fall below that of the surrounding warmer layer. Although this is not the situation in the clouds we consider (there are many different coolants, and different coolants operate at different depths; FFJ assumed one-sided illumination), the geometry does occur in parts of the flow.

We did tests to simulate the two-sided illuminated case. In this case the cloud core 'sees' both the part of the layer we model, and also a mirror image that is symmetric about the core. The main effect is that the total line optical depths are twice as large as those to the mid-plane – at the core the line optical depth is the same in all directions and equal to the optical depth from the illuminated face to the shielded face in the previous calculations.

The predicted structure is shown as the triple-dotted-dashed line in Fig. 6. As expected, the clouds are indeed slightly warmer. The main coolant in the core is CO, and Table 1 shows that, although the intensity of the lowest $1-0$ transition hardly changes, the higher rotation lines become somewhat brighter. As the lower J lines become more optically thick their upper level population increases, and higher transitions in the rotation ladder carry the

Table 1. Emission line strengths, relative to Hβ, predicted from the irradiated cloud models. Column 1 gives the line identifier while column 2 shows the wavelength of the line. Columns 3–7 give the line intensities relative to Hβ for the cloud irradiated from one side, the cloud with $1\,\mathrm{km\,s^{-1}}$ microturbulence, the dusty cloud, the cloud irradiated from two sides, and the dusty cloud where the temperature was not allowed to fall below 30 K, respectively. The surface flux of the Hβ line in units of $\mathrm{erg\,cm^{-2}\,s^{-1}}$ is given for each model at the bottom.

Line		One side	Turbulence	Dust	Two side	Heat + dust
Hα	6563 Å	5.42	5.53	4.21	5.41	4.24
Pα	1.87 μm	0.88	0.87	0.43	0.88	0.84
He I	626 Å	9.68	0.56	1.49	9.68	–
[C I]	609 μm	11.7	23.3	9.33	11.1	22.9
[C I]	369 μm	28.4	20.9	23.2	25.6	58.5
[C II]	157 μm	3.33	2.43	1.3	3.35	1.45
[O I]	63.1 μm	12.8	12.5	38.8	12.8	39.8
[O I]	145 μm	0.43	0.43	2.09	0.43	2.04
[Si II]	34.8 μm	15.00	15.5	2.48	15.00	2.34
[Fe II]	25.9 μm	1.44	1.48	0.09	1.45	–
$^{12}\mathrm{C}^{16}\mathrm{O}$	1–0	0.14	–	–	0.13	0.47
	2–1	0.88	0.84	0.02	0.87	4.67
	3–2	2.18	3.5	0.16	2.28	13.1
	4–3	3.02	5.43	0.20	3.42	15.3
	5–4	2.29	1.59	0.11	3.46	7.99
	6–5	0.34	0.02	0.05	1.32	1.92
$^{13}\mathrm{C}^{16}\mathrm{O}$	3–2	0.1	0.22	0.01	0.14	0.69
	4–3	0.21	0.5	–	0.38	0.55
	5–4	0.13	0.04	–	0.35	0.19
Hβ	Flux	1.73E−7	1.56E−7	7.23E−8	1.73E−7	7.62E−8

cooling. These lines, which are the most efficient coolants, have small optical depths.

4.5 A heated cloud with dust

Galactic molecular clouds are not heated by starlight photoionization. Rather a variety of agents, many involving mechanical or magnetic processes, act to sustain the temperature at higher-than-expected levels. Were this to occur in the clouds we computed, the CO would be stronger than we predict.

As a test we recomputed our dusty (zero-turbulence) model, but not allowing the temperature to fall below 30 K. The full thermal solution was performed when the equilibrium temperature was found to be above this limit, but a constant 30 K temperature was used for gas that otherwise would have been cooler. The results are given in the final column of Table 1.

The hydrogen lines are fainter because of absorption of the incident continuum by grains, and the Si and Fe lines are fainter because of depletion of these elements on to grains. The C I lines, and especially the CO rotation transitions, are, however, stronger. This is caused by the warmer temperature in regions where they are formed. Actually, the CO lines could increase in intensity, almost without limit, were the cloud column density to be increased (the calculation was stopped at a somewhat arbitrary depth). The important results are the line ratios.

4.6 Observational evidence for molecular gas and dust in cooling flows

Until recently, there was little evidence for cold molecular gas in cooling flows. NGC 1275 in the centre of the Perseus cluster had been detected (Bridges & Irwin 1998) and many non-detections reported (Grabelsky & Ulmer 1990; McNamara & Jaffe 1992; Braine & Dupraz 1994; O'Dea et al. 1994; Henkel & Wiklind 1997). Now CO line emission has been found in the central galaxies of 16 central cluster galaxies (Edge 2001). The molecular gas implied by

these detections has a temperature consistent with 20–40 K and masses that range from $10^9\,\mathrm{M_\odot}$ in the weakest objects to $10^{11.5}\,\mathrm{M_\odot}$ in the strongest. More cooler gas could be present; the CO flux predicted by our standard model from a square kpc of our irradiated clouds is less than 1 per cent of that detected by Edge (2001). Smaller masses of much hotter molecular gas have also been found in cooling flows through vibrational H$_2$ emission (Jaffe & Bremer 1997; Falcke et al. 1998; Donahue et al. 2000; Jaffe, Bremer & van der Werf 2001; Edge et al. 2002; Wilman et al. 2002).

Dust also appears to be common in this environment, and is detected either by its effect on emission-line ratios (Hu 1992; Donahue & Voit 1993; Allen et al. 1995; Allen 1995; Hansen, Jorgensen & Norgaard-Nielsen 1995; Crawford et al. 1999), dust lanes (Sparks, Macchetto & Golombek 1989; McNamara et al. 1996; Pinkney et al. 1996) or FIR/submillimetre emission (Lester et al. 1995; Cox, Bregman & Schombert 1995; Allen et al. 2001; Edge 2001; Irwin, Stil & Bridges 2001).

The origin and heating of the molecular gas and grains is currently unknown. They may form from gas cooled from the cooling intracluster medium and be enriched and photoionized by the emissions of massive young stars formed within the cooled clouds, or they may have another source. This uncertainty also remains for the optical nebulosity common in cooling flows. The cold clouds modelled in this paper would only be detectable in emission if they were both dust-free and had a covering fraction exceeding 10 per cent over the telescope beam (scaling from the results of Edge 2001). Such a high covering fraction would imply a molecular mass greater than $10^{11}\,\mathrm{M_\odot}$ for objects at $z \sim 0.1$ and the instruments used by Edge (2001). However, part of the emission seen may be caused by the clouds modelled here. Detection by absorption would, of course, depend on the covering factor and velocity spread of the cloud population.

4.7 The H I 21-cm line

There is atomic hydrogen in our models, suggesting that the clouds

might be observed, in absorption or emission, through the H I 21-cm line. Indeed, a number of detections have been made (see, e.g., Allen 2000 for references).

Lines at radio wavelengths are characterized by their brightness temperatures, which will be nearly equal to the spin temperature of the line at the position where it reaches an optical depth of roughly unity. The clouds we model are quite optically thick in the 21-cm line ($\tau \sim 10^3$ for the standard cold cloud computed here) so the observed brightness temperature will depend on which side of the cloud is viewed. An observer viewing the cloud from its illuminated face would see a brightness temperature of $\sim 15\,\mathrm{K}$, while an observer viewing the shielded side would see a slightly lower temperature, nearer $10\,\mathrm{K}$. Note that these would be the observed brightness temperatures if the clouds fully fill the beam of the telescope. If the clouds do not fill the beam the observed brightness temperature will be lower as the remainder of the beam sees the cosmic microwave background. Our model makes no prediction for the cloud filling factor.

5 SUMMARY

We have shown that a pressure-confined cloud at a radius of $\sim 100\,\mathrm{kpc}$ in a cooling flow irradiated by a cooling flow has a large cold core at a temperature of less than $17\,\mathrm{K}$, where cooling by atomic carbon is dominant. This coolant explains the major difference between our result and that obtained using molecular cloud cooling rates by O'Dea et al. (1994) and others. Clouds with a small amount of microturbulence, or dust, are colder still. The temperature profile of the dusty cloud drops very rapidly towards that of the microwave background.

Owing to the continuing revisions of the atomic and molecular cross-sections, rates and processes that have taken place since FFJ, there have been changes in our computed model that we have explored in detail. Further small changes will probably occur over the next few years.

We do not argue here that such clouds necessarily are the sink of the cooled matter in cooling flows, or are the source of the excess X-ray absorption inferred in their spectra. That will be explored elsewhere. Our purpose has been to confirm, from a detailed calculation of the thermal and radiation balance of X-ray-irradiated and pressure-confined gas, that very cold clouds can be expected in the cooling flow environment.

REFERENCES

Allen C. W., 1973, Astrophysical Quantities, 3rd edn. The Athlone Press, Univ. London
Allen S. W., 1995, MNRAS, 276, 947
Allen S. W., 2000, MNRAS, 315, 269
Allen S. W., Fabian A. C., Edge A. C., Böhringer H., White D. A., 1995, MNRAS, 275, 741
Allen S. W., Fabian A. C., Johnstone R. M., Arnaud K. A., Nulsen P. E. J., 2001, MNRAS, 322, 589
Bertoldi F., Draine B. T., 1996, ApJ, 458, 222
Braine J., Dupraz C., 1994, A&A, 283, 407
Braine J., Wyrowski F., Radford S. J. E., Henkel C., Lesch H., 1995, AaA, 283, 315
Bridges T. J., Irwin J. A., 1998, MNRAS, 300, 967
Cox C. V., Bregman J. N., Schombert J. M., 1995, ApJS, 99, 405
Crawford C. S., Edge A. C., Fabian A. C., Allen S. W., Bohringer H., Ebeling H., McMahon R. G., Voges W., 1995, MNRAS, 273, 827
Crawford C. S., Allen S. W., Ebeling H., Edge A. C., Fabian A. C., 1999, MNRAS, 306, 857
Crosas M., Weisheit J. C., 1993, MNRAS, 262, 359
Dalgarno A., Yan M., Liu W., 1999, ApJS, 125, 237
de Jong T., Chu S-I., Dalgarno A., 1975, ApJ, 199, 69
Donahue M., Voit G. M., 1993, ApJ, 414, L17
Donahue M., Mack J., Voit G. M., Sparks W., Elston R., Maloney P. R., 2000, ApJ, 545, 670
Draine B. T., Bertoldi F., 1996, ApJ, 468, 269
Dufton P. L., Kingston A. E., 1994, ADNDT, 57
Edge A. C., 2001, MNRAS, 328, 762
Edge A. C., Wilman R. J., Johnstone R. M., Crawford C. S., Fabian A. C., Allen S. W., 2002, MNRAS, submitted
Elitzur M., Ferland G. J., 1986, ApJ, 305, 35
Fabian A. C., Johnstone R. M., Daines S. J., 1994, MNRAS, 266, 411
Falcke H., Rieke M. J., Rieke G. H., Simpson C., Wilson A. S., 1998, ApJ, 494, L155
Ferland G. J., Fabian A. C., Johnstone R. M., 1994, MNRAS, 271, 737 (FFJ)
Ferland G. J., Korista K. T., Verner D. A., Ferguson J. W., Kingdon J. B., Verner E. M., 1998, PASP, 110, 761
Goldsmith P. F., Langer W. D., 1978, ApJ, 222, 881
Grabelsky D. A., Ulmer M. P., 1990, ApJ, 355, 401
Guhathakurta P., Draine B. T., 1989, ApJ, 345, 230
Hansen L., Jorgensen H. E., Norgaard-Nielsen H. U., 1995, A&A, 297, 13
Henkel C., Wiklind T., 1997, SSRev, 81, 1
Hollenbach D., McKee C. F., 1979, ApJS, 41, 555
Hollenbach D., McKee C. F., 1989, ApJ, 342, 306
Hollenbach D. J., Tielens A. G. G. M., 1999, Rev. Mod. Phys., 71, 173
Hu E. M., 1992, ApJ, 391, 608
Irwin H. A., Stil J. M., Bridges T. J., 2001, MNRAS, 328, 359
Jaffe W., Bremer M. N., 1997, MNRAS, 284, L1
Jaffe W., Bremer M. N., van der Werf P. P., 2001, MNRAS, 324, 443
Johnstone R. M., Fabian A. C., Nulsen P. E. J., 1987, MNRAS, 224, 75
Johnstone R. M., Fabian A. C., Taylor G., 1998, MNRAS, 298, 854
Lenzuni P., Chernoff D. F., Salpeter E. E., 1991, ApJS, 76, 759
Lester D. F., Zink E. C., Doppmann G. W., Gaffney N. I., Harvey P. M., Smith B. J., Malkan M., 1995, ApJ, 439, 185
Kaastra J. S., Mewe R., 1993, AAS, 97, 443
Kurucz R. L., 1991, in Philip A. C. D., Upgren A. R., James K. A., eds, Proc. Workshop on Precision Photometry, Astrophysics of the Galaxy. Davis, Schenectady, p. 27
McNamara B. R., Jaffe W., 1994, A&A, 281, 673
McNamara B. R., Wise M., Sarazin C. L., Jannuzi B. T., Elston R., 1996, ApJ, 466, L9
Maloney P. R., Hollenbach D. J., Tielens A. G. G. M., 1996, ApJ, 466, 561
O'Dea C. P., Baum S. A., Maloney C. P., Tacconi L. J., Sparks W. B., 1994, ApJ, 422, 467
Pinkney J. et al., 1996, ApJ, 468, L13
Puy D., Alecian G., Le Bourlot J., Leorat J., Pineau des Forets G., 1993, A&A, 267, 337
Puy D., Grenacher L., Jetzer P., 1999, A&A, 345, 723
Reilman R. F., Manson S. T., 1979, ApJS, 40, 815
Seaton M. J., 1987, J Phys B, 20, 6363
Shull J. M., van Steenberg M. E., 1985, ApJ, 298, 268
Sparks W. B., Macchetto F., Golombek D., 1989, ApJ, 343, 153
Tielens A. G. G. M., Hollenbach D., 1985a, ApJ, 291, 722
Tielens A. G. G. M., Hollenbach D., 1985b, ApJ, 291, 746
van Dishoeck E. F., Black J. H., 1988, ApJ, 334, 771
van Hoof P. A. M., Weingartner J. C., Martin P. G., Volk K., Ferland G. J.,

2001, in Ferland G., Savin D., eds, ASP Conf. Ser., Challenges of Photoionized Plasmas. Astron. Soc. Pac., San Francisco in press (astro-ph/0107183)

Verner D., Ferland G. J., Korista K., Yakovlev D. G., 1996, ApJ, 465, 487

Voit G. M., Donahue M., 1995, ApJ, 452, 164 (VD)

Weingartner J. C., Draine B. T., 2001, ApJS, 134, 263

Weisheit J. C., 1974, ApJ, 190, 735

Weisheit J. C., Collins L. A., 1976, ApJ, 210, 299

Wilman R. J., Edge A. C., Johnstone R. M., Fabian A. C., Allen S. W., Crawford C. S., 2002, MNRAS, submitted

Weisheit J. C., Dalgarno A., 1972, Ap. Lett., 12, 103

Wolfire M. G., Tielens A., Hollenbach D., 1990, ApJ, 358, 116

Xu Y., McCray R., 1991, ApJ, 375, 190

Zhang H. L., Pradhan A., 1995, AaA, 293, 953

This paper has been typeset from a TEX/LATEX file prepared by the author.